Physics Letters A 380 (2016) 3748–3755

Contents lists available at ScienceDirect

Physics Letters A

www.elsevier.com/locate/pla

Anisotropic electrical and lattice transport properties of ordered quaternary phases Cr_2TiAlC_2 and Mo_2TiAlC_2: A first principles study

Y.F. Li [a], Y.C. Ding [b], B. Xiao [c,*], Y.H. Cheng [d]

[a] State Key Laboratory for Mechanical Behavior of Materials, Xi'an Jiaotong University, Xi'an 710049, China
[b] College of Optoelectronics Technology, Chengdu University of Information Technology, Chengdu, 610225, China
[c] Department of Earth Sciences, University College London, London, WC1E 6BT, England, United Kingdom
[d] State Key Laboratory of Electric Insulation and Power Equipment, Xi'an Jiaotong University, Xi'an 710049, China

ARTICLE INFO

Article history:
Received 13 August 2016
Received in revised form 31 August 2016
Accepted 14 September 2016
Available online 19 September 2016
Communicated by M. Wu

Keywords:
Cr_2TiAlC_2 and Mo_2TiAlC_2
Electrical conductivity
Thermal conductivity
Thermoelectric property

ABSTRACT

Electrical conductivities of Cr_2TiAlC_2 and Mo_2TiAlC_2 in *a* and *c* directions are calculated from semi-classic Boltzmann transport theory. The values are found to be $\sigma_a = 5.68 \times 10^5$ S/m (6.56×10^5 S/m) and $\sigma_c = 2.15 \times 10^5$ S/m (2.69×10^5 S/m) for Cr_2TiAlC_2 (Mo_2TiAlC_2) at 300 K. Using the phonon-mode Debye temperature and Slack-model, the lattice thermal conductivities in the two directions are also evaluated, and the values are $\kappa_a = 18.71$ W/m K (16.11 W/m K) and $\kappa_c = 0.48$ W/m K (0.25 W/m K) for Cr_2TiAlC_2 (Mo_2TiAlC_2) at room temperature. The anisotropy in lattice thermal conductivity is found to be stronger than that of electrical conductivity. The predicted Seebeck coefficients and thermoelectric figure of merit (ZT) indicate that they are poor thermoelectric materials. Due to the relatively high conductivities, they might be used to fabricate high temperature conductive components in aerospace industry. In addition, our results in *a* direction have the direct implications for the relevant properties of MXenes (Cr_2TiC_2 and Mo_2TiC_2), produced from their bulk phases.

1. Introduction

Titanium aluminum carbide (Ti_3AlC_2) is one of the most known $M_{n+1}AX_n$ phases, which belongs to a family of layered ternary compounds, has been attracting considerable attention owing to its unique combinative properties of both metals and ceramics in recent years [1–6]. Like metals it is thermally and electrically conductive, easy to be machined with conventional tools and resistant to thermal shock. Like ceramics it has low density, high elastic modulus, excellent creep and oxidation resistance [7,8]. The combination of these remarkable properties makes Ti_3AlC_2 a great candidate for applications as the lightweight and high temperature structural materials.

In order to improve the mechanical and electrical properties of Ti_3AlC_2 further, some quaternary MAX phases have also been synthesized, e.g., Cr_2TiAlC_2 and Mo_2TiAlC_2. In these quaternary phases, double transition metal ordered MAX phase are formed, and Cr/Mo layers are directly bonded to Al atoms. Recently, Liu et al. [9] reported on synthesizing Cr_2TiAlC_2 by reacting Cr_2AlC and TiC. Based on their neutron diffraction and Raman spectroscopy, they claimed that the Cr_2TiAlC_2 possesses an M ordered M_3AX_2 phase structure with Ti and Cr occupying 2a and 4f Wyckoff sites, respectively. More recently, Anasori et al. [10] reported on a new Mo-containing ordered M_3AX_2 phase, Mo_2TiAlC_2, which was synthesized by heating an elemental mixture of Mo, Ti, Al, and graphite at 1600 °C for 4 h under an argon flow. It was found that Mo_2TiAlC_2 is isostructural with Cr_2TiAlC_2. In a latter paper of the same group [11], the electrical resistivity was measured below 300 K for Mo_2TiAlC_2, and which showed typical behavior of a conductive metallic phase. The calculated band structures and electronic density of states completely supported the electrical measurement [11].

Up to now, there is lack of information about the thermal and electrical transport properties of those two newly discovered ordered quaternary MAX phases Cr_2TiAlC_2 and Mo_2TiAlC_2. Certainly, we consider transport properties of them are important for their applications as high temperature structural materials, electrical contacts, heating elements, heat exchanger and additives in the tribological practice [1,12]. Furthermore, the thermoelectric properties of bulk MAX phases are little known at the moment. The transport and thermoelectric properties of bulk Cr_2TiAlC_2 and Mo_2TiAlC_2 phases also have great implications for their corresponding two-dimensional (2D) materials MXenes [1,13–16].

* Corresponding author.
E-mail addresses: b.xiao@ucl.ac.uk, xbaprs@163.com (B. Xiao).

http://dx.doi.org/10.1016/j.physleta.2016.09.015
0375-9601/

In present work, we report a comprehensive theoretical investigation of those parameters of Cr_2TiAlC_2 and Mo_2TiAlC_2 for the first time.

2. Calculation method and details

Crystal structures of Cr_2TiAlC_2 and Mo_2TiAlC_2 were optimized using density functional theory as available in *Cambridge Serial Total Energy Package* (CASTEP) [17]. The norm conserving pseudopotentials were employed to describe the Coulomb interactions between the valence electrons and pseudo-ion core. The kinetic energy cut-off value of 950 eV was used for plane wave expansion in reciprocal space. The valence electrons were treated as: Cr: $3d^5 4s^1$, Mo: $4d^5 5s^1$, Ti: $3d^2 4s^2$, Al: $3s^2 3p^1$, C: $2s^2 2p^2$, respectively. The sampling k-point mesh in the first irreducible Brillouin zone (BZ) was generated by Monkhorst–Pack method [18], using a $6 \times 6 \times 1$ grid for all studied structures. The convergence criterion were: 10^{-8} eV/atom in energy and 5×10^{-5} eV/Å in atomic force. The exchange-correlation density functional was treated within Perdew–Burke–Ernzerhof (PBE) of generalized gradient approximation (GGA) [19]. The phonon frequencies at the boundary of Brillouin zone were calculated by employing the standard density functional perturbation theory (DFPT) in the same code. The dynamical matrices at given q points in first Brillouin zone can be obtained from the Fourier interpolation algorithm, the quality of the q factor spacing was set to 0.01 $Å^{-1}$, and the BZ path was set as $M(0\ 0.5\ 0)-\Gamma(0\ 0\ 0)-A(0\ 0\ 0.5)$. This path allows us to study the anisotropic properties along two principal directions ([010] and [001] axes) of phonon spectrum and other derived parameters straightforwardly.

The electrical conductivity tensor components were calculated using BoltzTrap code [20], i.e., solving the semi-classic Boltzmann transport equation with the constant relaxation time approximation. In order to apply BoltzTrap to our structures, the band structures of them were recalculated in *Vienna Ab initio Simulation Package* (VASP) [21–23]. We employed 500 eV for kinetic energy cut-off value. The exchange-correlation density functional and valence electron configurations of the elements were the same as those given in the above section. The k-gird used in structural and energy calculations was $20 \times 20 \times 8$, generated by Γ-point centered method for hexagonal symmetry. For computing the band structure, we used a finer k-gird as $20 \times 20 \times 16$. The obtained band structures of Cr_2TiAlC_2 and Mo_2TiAlC_2 then processed by BoltzTrap code to obtain all non-zero components of electrical conductivity tensor.

BoltzTrap calculates the electrical conductivity as a two-dimensional function of both temperature (T) and chemical potential (μ_e). In this work, we only report the results for $\mu_e = 0.10$ eV (or 0.01 Ry). The value is equivalent to the highest temperature considered in the calculation, i.e., 1400.0 K. Since the quantity like electrical conductivity is given as σ/τ_0 in BoltzTrap code ($\tau_0 = 1$ fs), the results must be rescaled by a carefully determined relaxation time (τ) to obtain more realistic values ($\sigma\tau/\tau_0$). We used $\tau = 2.0 \times 10^{-15}$ s throughout all calculations. Using this optimized relaxation time, it is found that the predicted electrical conductivity of Mo_2TiAlC_2 is in close agreement with experimental value at 300 K. Since the electrical conductivity of Cr_2TiAlC_2 phase has not been reported experimentally before, the relaxation time was fixed to that of Mo_2TiAlC_2. Moreover, a rigorous estimation of relaxation time is highly non-trivial [24]. Such attempt was not conducted in current paper. The uncertainty in the calculated electrical conductivity of Cr_2TiAlC_2 phase is considered to be acceptable, because the electronic states near the Fermi level of the two structures are similar to each other [9,11], i.e., both are dominated by d states. Therefore, the average relaxation time in Cr_2TiAlC_2 phase is expected to be not very different to Mo_2TiAlC_2.

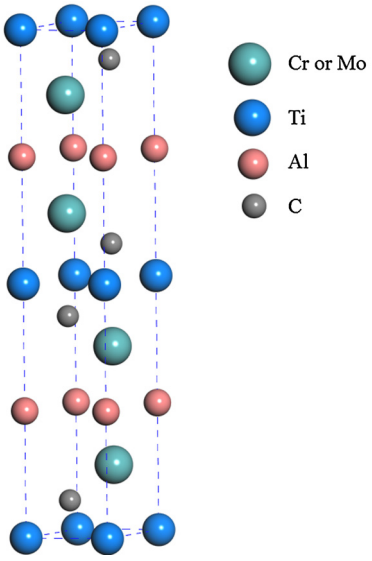

Fig. 1. Crystal structure of fully ordered M_2TiAlC_2 (M = Cr or Mo).

3. Results and discussions

M_2TiAlC_2 (M = Cr or Mo) phases have hexagonal structure ($P6_3mc$), and the conventional cell, which has two formula units ($2f.u.$), is shown in Fig. 1. The optimized atomic coordinates and lattice parameters of Cr_2TiAlC_2 and Mo_2TiAlC_2 are shown in Table 1. The calculated results are consistent with the experimental data given in Refs. [9–11]. The phonon spectra and electronic band structures of them are depicted in Fig. 2. The soft phonon modes are not observed in the phonon spectra, implying that both structures are dynamically stable. On the other hand, the band structures are dominated by d states of Cr or Mo at Fermi level. Similar results have been reported before in other works for MAX phases [2,10,25,26]. Interestingly, Cr_2TiAlC_2 is metallic in M–K direction in Brillouin zone. In contrast, Mo_2TiAlC_2 has a band gap in the same k-path. Band dispersions below the Fermi level are very similar to each other.

The results of electrical conductivities in a and c crystallographic directions are illustrated in Fig. 3 as a function of temperature between 300 K and 1400 K for Cr_2TiAlC_2 and Mo_2TiAlC_2. As can be seen from Fig. 3, Mo_2TiAlC_2 has larger electrical conductivities in both a and c directions than those of Cr_2TiAlC_2. This can be explained from their electronic structures, as displayed in Fig. 2. It can be seen that 4d states of Mo are more delocalized in space than those of Cr (3d), leading to more dispersive 4d electronic bands in former phase. Therefore, Mo_2TiAlC_2 is more conductive than Cr_2TiAlC_2. The experimental electrical conductivity of Mo_2TiAlC_2 was reported as 4.79×10^5 S/m at 300 K in Ref. [10]. This value is significantly larger than σ_c (2.69×10^5 S/m), but it is close to σ_a (6.56×10^5 S/m) at the same temperature. Certainly, experimental value is fairly in agreement with the average value ($(2\sigma_a + \sigma_c)/3 = 5.27 \times 10^5$ S/m). The experimental electrical conductivities of Ti_3AlC_2, Ti_3SiC_2 and Ti_4AlN_3 were found to be 3.6×10^5 S/m, 2.2×10^5 S/m and 4.3×10^6 S/m at 300 K in Ref. [2]. Electrical conductivities of M_2TiAlC_2 (M = Cr or Mo) seem to be larger than their parent structure Ti_3AlC_2. This is consistent with the fact that Cr and Mo have more electrons in d states than Ti.

The anisotropy in electrical conductivity tensor is clearly displayed in Fig. 4. The two-dimensional polar plots are obtained by Eq. (1).

$$\sigma(\theta) = \sigma_{xx} \sin^2(\theta) + \sigma_{zz} \cos^2(\theta) \tag{1}$$

Table 1
The calculated atomic fractional coordinates, lattice parameters, equilibrium cell volume and density (a, c, in Å; V_0 in Å^3; ρ in g/cm^3) of M_2TiAlC_2 (M = Cr, Mo). For each structure, data in the first row refer to CASTEP results; VASP values are given the second row.

Compounds	Atomic positions[a]		Lattice parameters		V_0	ρ
	u	v	a	c		
Cr_2TiAlC_2	0.1335	0.0746	2.923	17.634	130.447	5.166
	0.1329	0.0754	2.904	17.781	129.875	5.188
	(0.131[b])	(0.07[b])	(2.906[b], 2.93[c])	(17.803[b], 17.83[c])	(130.201[b])	(5.175[b])
Mo_2TiAlC_2	0.1347	0.0676	3.014	18.651	146.712	6.582
	0.1338	0.0687	3.001	18.711	145.964	6.617
	(0.1333[d])	(0.0688[d])	(2.997[d], 2.999[e])	(18.661[d], 18.759[e])	(145.157[d], 146.09[e])	(6.653[d])

[a] Atomic positions in M_2TiAlC_2 are 4f (2/3, 1/3, u) for Cr (Mo), 2a (0, 0, 0) for Ti, 2b (0, 0, 1/4) for Al and 4f (1/3, 2/3, v) for C, respectively.
[b] Exp. data from Liu et al. [9].
[c] Cal. lattice parameters from Ref. [25].
[d] Exp. data from Anasori et al. [10,11].
[e] Cal. data by Gao et al. [26].

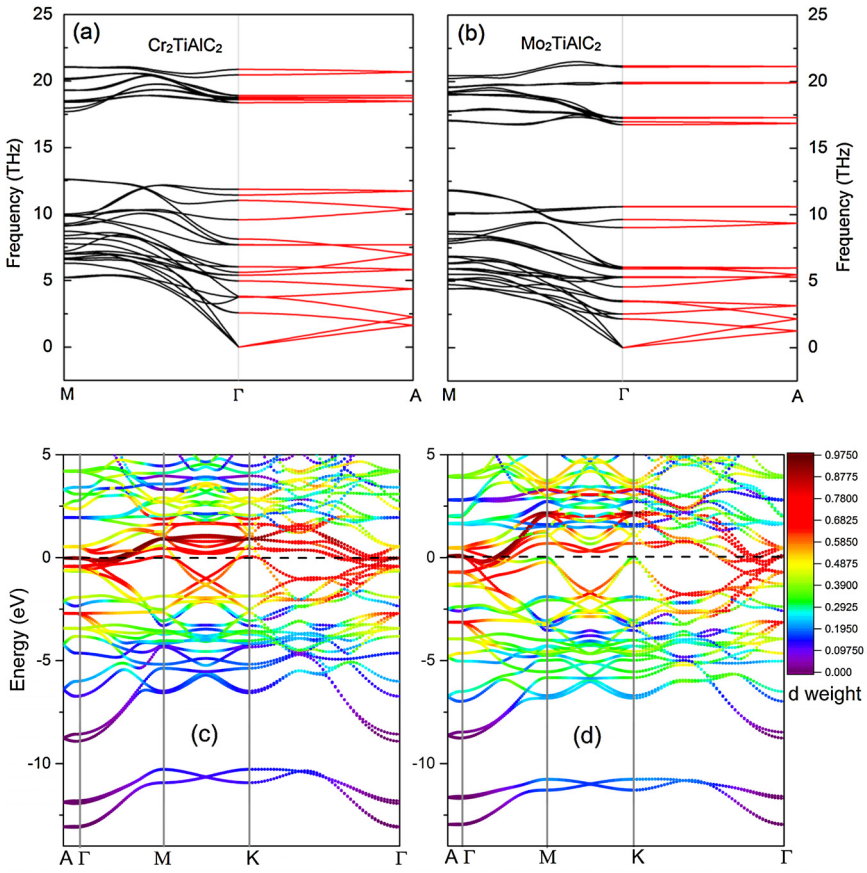

Fig. 2. The phonon dispersions and electronic band structures of Cr_2TiAlC_2 ((a) and (c)) and Mo_2TiAlC_2 ((b) and (d)) at their equilibrium cell volumes. In phonon spectrum, the special k-path in the Brillouin zone is $M(0\ 0.5\ 0]-\Gamma(0\ 0\ 0)-A(0\ 0\ 0.5)$. Meanwhile, the k-path for electronic bands is $A(0\ 0\ 0.5)-\Gamma(0\ 0\ 0)-M(0\ 0.5\ 0)-K(0.5\ 0.5\ 0)-\Gamma(0\ 0\ 0)$. The color map indicates the weight of d states of Cr or Mo atoms at each k point. The horizontal dashed line refers to Fermi level. (For interpretation of the references to color in this figure legend, the reader is referred to the web version of this article.)

In Eq. (1), the polar angle between [001] and another arbitrary crystallographic directions is denoted as θ. From Fig. 4, one can see that Mo_2TiAlC_2 exhibits a slightly stronger anisotropic contour than that of Cr_2TiAlC_2, and which is consistent with the ratio σ_a/σ_c (2.7 for Cr_2TiAlC_2 and 2.5 for Mo_2TiAlC_2) at 300 K.

Lattice thermal conductivity is needed to evaluate thermoelectric property, i.e., figure of merit (ZT) [27]. In this paper, we calculate lattice thermal conductivities in a and c crystallographic directions using the modified Slack model [28,29], as shown in Eq. (2).

$$k = A\frac{\overline{M}\langle\Theta_a\rangle^3\delta n^{1/3}}{\gamma^2(T)T} \tag{2}$$

Here, the constant A is computed as $A = 2.43\times10^4/(1 - 0.514/\gamma + 0.228/\gamma^2)$ [30]. $\overline{M}$ is the average mass per atom of the cell; δ refers to the average size of the atom in the cell; n is the number of atoms in the primitive unit cell, $\gamma(T)$ represents the macroscopic Grüneisen parameter, averaged over all phonon-mode Grüneisen constants in Brillouin zone along a principal crystallographic direction [28]. It is computed by Eq. (3):

$$\gamma(T) = \frac{\sum_i C_V(\omega_i, T)\gamma(\omega_i)}{\sum_i C_V(\omega_i, T)} \tag{3}$$

In Eq. (3), the mode-specific heat is denoted as $C_V(\omega_i, T)$. In many previous works [31–34], it has been shown that acoustic

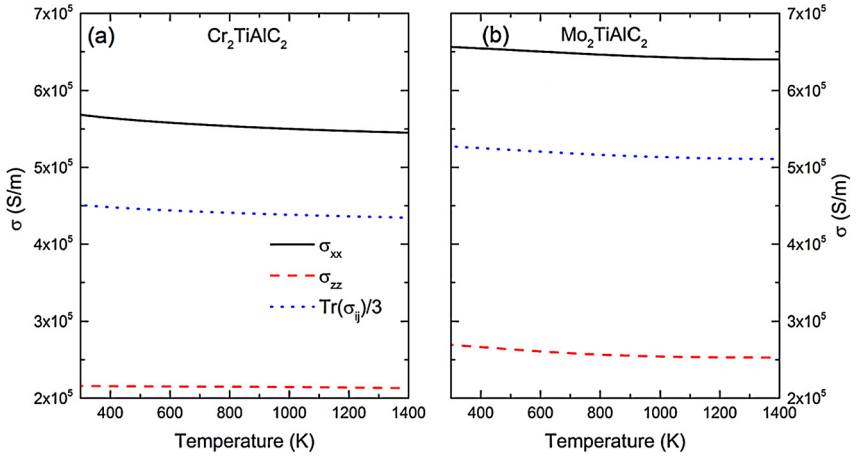

Fig. 3. Electrical conductivities in a and c directions between 300 K and 1400 K of (a): Cr_2TiAlC_2 and (b): Mo_2TiAlC_2. The average is also shown in each case.

phonon branches play the dominant role in the lattice heat transfer. Based on this observation, mode-Debye temperature was defined in Refs. [28] and [35] to evaluate lattice thermal conductivity empirically. In this work, similar to Ref. [28], the mode-averaged Debye temperature is denoted as $\langle\Theta_a\rangle$, and which is defined in Eq. (4).

$$\frac{1}{\langle\Theta_a\rangle} = \left[\frac{1}{3}\left(\frac{1}{(\Theta_{LA})^3} + \frac{1}{(\Theta_{TA1})^3} + \frac{1}{(\Theta_{TA2})^3}\right)\right]^{1/3} \tag{4}$$

In Eq. (4), *TA* and *LA* refer to transverse and longitudinal acoustic phonon modes. The mode-Debye temperature is evaluated as $\Theta_i = \hbar\omega_i/k_B$, with k_B Boltzmann constant and $\hbar$ the reduced Planck constant. The phonon frequencies (ω_{LA}, ω_{TA1} and ω_{TA2}) are defined as the maximum values in three acoustic phonon dispersions along a principal direction, i.e., [001] and [100] directions [18,35]. Usually, a good approximation is simply to use the phonon frequencies of three acoustic branches at the boundary of Brillouin in the corresponding direction. Phonon spectra of Cr_2TiAlC_2 and Mo_2TiAlC_2 in two principal crystallographic directions are given in Fig. 2. Phonon mode-Debye temperatures used in our calculations are listed in Table 2. In both MAX phases, Debye temperature in c direction is roughly three times smaller than that of a direction. From Eq. (2), one can see that the low Debye temperature implies a small lattice thermal conductivity in the direction. This is indeed what we have observed from the calculated lattice thermal conductivities in a and c directions, as shown in Table 2. In Fig. 5, we display the temperature dependence of lattice thermal conductivity (κ_l) of M_2TiAlC_2 (M = Cr or Mo) between 300 K and 1400 K. As Eq. (2) suggested, the lattice thermal conductivity decreases as $1/T$ with the increasing of temperature. This is reasonable, because the main phonon scattering mechanism above Debye temperature is the three-phonon Umklapp processes (U-process). Overall, lattice thermal conductivity of Cr_2TiAlC_2 is larger than that of Mo_2TiAlC_2. At 300 K, the anisotropic factor $\kappa_a/\kappa_c = 38.90$ for Cr_2TiAlC_2 and that value is 64.4 for Mo_2TiAlC_2. The ratio is larger in latter structure, because the atomic mass of Mo is much heavier than that of Cr. The presence of large atomic mass contrast in the crystal structure is regarded as an effective strategy to suppress the lattice heat transfer [36,37]. The average lattice thermal conductivities are found to be 15.9 W/m K and 14.9 W/m K for Cr_2TiAlC_2 and Mo_2TiAlC_2 between 300 K and 1400 K, respectively.

The electrical thermal conductivity (κ_e) can be obtained from Wiedemann–Franz law, using the calculated electrical conductivity. The total thermal conductivity is computed as $\kappa_t = \kappa_l + \kappa_e$. The values of electrical thermal conductivity at 300 K are also given

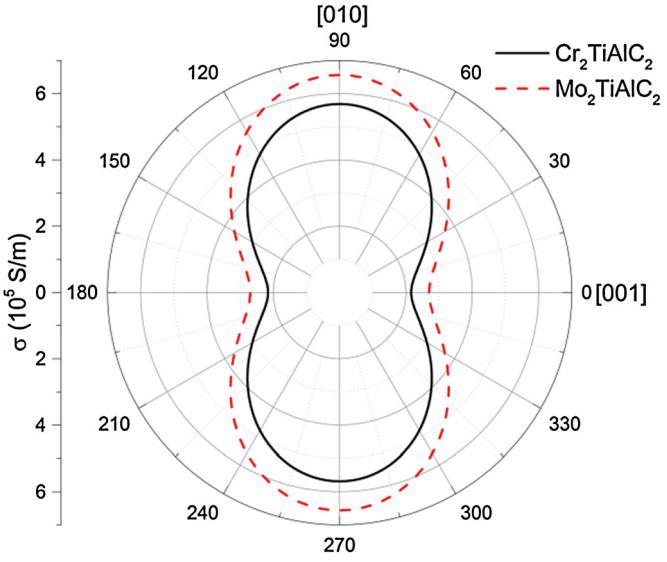

Fig. 4. Anisotropic electrical conductivity of M_2TiAlC_2 (M = Cr or Mo) phases at 300 K.

Table 2
Mode-Debye temperatures and their averages of three acoustic phonon branches in a and c directions. Typical values for transport properties are also shown in the same directions at 300 K.

Property	Cr_2TiAlC_2		Mo_2TiAlC_2	
Direction	a	c	a	c
Θ_{TA1} (K)	258.28	78.54	212.61	60.44
Θ_{TA2} (K)	260.10	78.54	214.55	60.44
Θ_{LA} (K)	302.60	89.40	227.31	73.51
$\langle\Theta_a\rangle$ (K)	270.86	81.57	217.78	63.76
κ_l (W/m K)	18.71	0.48	16.11	0.25
κ_e (W/m K)	4.03	1.57	4.75	1.89
κ_t (W/m K)	22.75	2.05	20.86	2.14
σ (10^5 S/m)	5.68	2.16	6.56	2.69

in Table 2 in a and c directions for M_2TiAlC_2 (M = Cr or Mo) structures. We plot κ_t, κ_l and κ_e in Fig. 6 in the two directions. Electronic thermal conductivity increases with the increasing of temperature, as opposite to that of lattice one. Interestingly, the total thermal conductivity in c direction is almost completely dominated by κ_e rather than κ_l at all temperatures. As a result, the obtained κ_t in c direction increases monotonically with tempera-

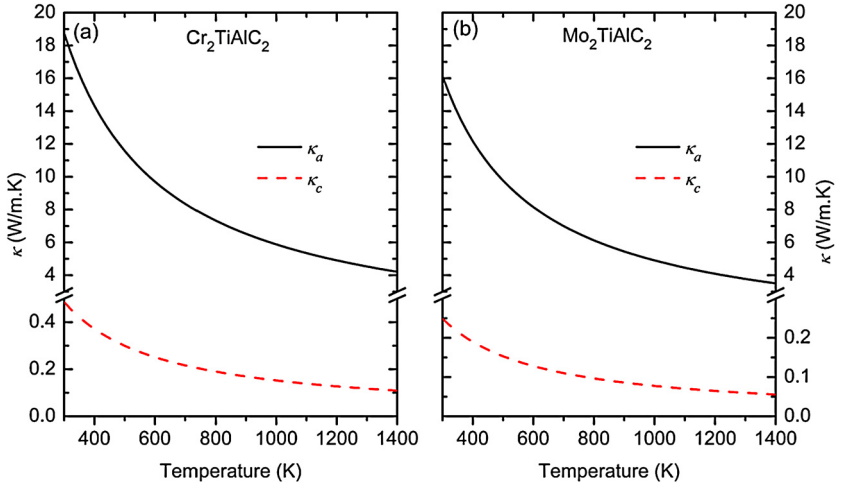

Fig. 5. Lattice thermal conductivities of Cr_2TiAlC_2 (a) and Mo_2TiAlC_2 (b) in a and c directions between 300 K and 1400 K.

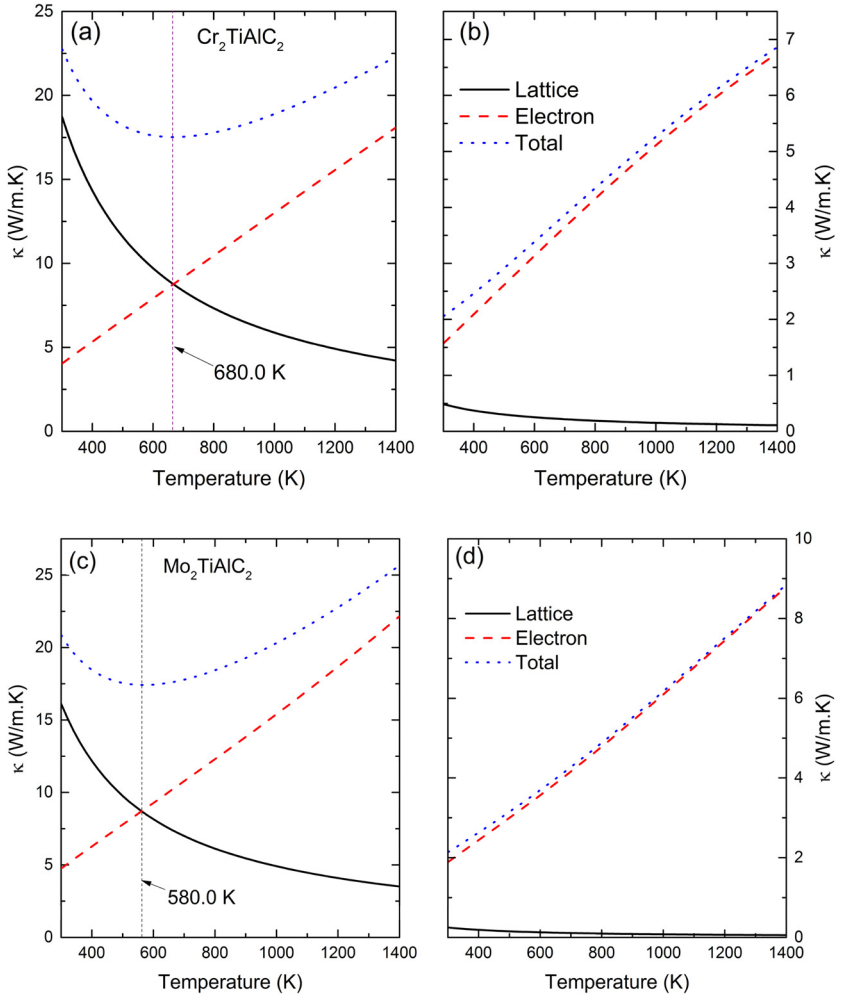

Fig. 6. Electrical, lattice and total thermal conductivities in a and c directions of Cr_2TiAlC_2 and Mo_2TiAlC_2 (a) and (c): a direction; (b) and (d): c direction. The dashed line indicates the turning point in total thermal conductivity where the minimum value is obtained.

ture. From Table 2, we can see the ratio κ_e/κ_l is 3.28 (7.86) for Cr_2TiAlC_2 (Mo_2TiAlC_2) even at 300 K in c direction. On the other hand, the decreasing of κ_l with T is compensated by the increasing of κ_e in a direction. The total thermal conductivity shows a turning point where the value reaches minimum. The temperature at this turning point is indicated in Fig. 6.

The anisotropy in thermal conductivities is illustrated in Fig. 7 at 300 K, using an expression similar to Eq. (1) for κ. We find that the anisotropy in κ_e is less prominent than that in κ_l at room temperature. Therefore, the contours of κ_l and κ_t are very similar to each other. At higher temperature, the contour of κ_t is expected to be determined by κ_e.

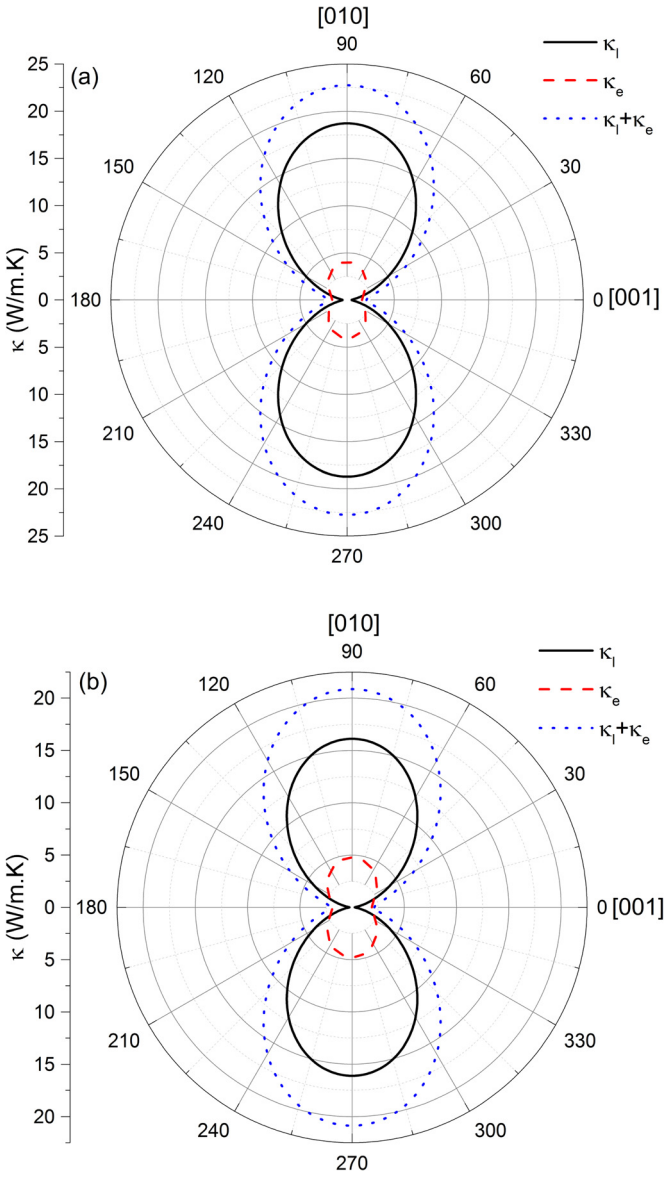

Fig. 7. Polar plots of thermal conductivities (κ_l, κ_e and κ_t) at 300 K. (a): Cr_2TiAlC_2; (b): Mo_2TiAlC_2.

Using the obtained electrical and lattice transport properties, we show the calculated Seebeck coefficients (S) and ZT values in Fig. 8 between 300 K and 1400 K. Thermoelectric figure of merit (ZT) is defined by Eq. (5) [35].

$$ZT = \frac{S^2 \sigma T}{\kappa} \tag{5}$$

For single crystal, we have $S = 2S_a + S_c$, $\sigma = 2\sigma_a + \sigma_c$, and $\kappa = 2\kappa_a + \kappa_c$. Meanwhile, for polycrystalline sample, the average Seebeck coefficient is evaluated as $S_{ave} = (2S_a\sigma_a + S_c\sigma_c)/(2\sigma_a + \sigma_c)$ [34]. Moreover, the average power factor (PF_{ave}) and mean thermal conductivity (κ_{ave}) are calculated first, then ZT is obtained from Eq. (5) for polycrystalline material. PF_{ave} and κ_{ave} are written as Eq. (6).

$$\left.\begin{aligned} PF_{ave} &= \frac{1}{3}(2S_a^2\sigma_a + S_c^2\sigma_c) \\ \kappa_{ave} &= \frac{1}{3}(2\kappa_a + \kappa_c) \end{aligned}\right\} \tag{6}$$

We should note that κ_a and κ_c refer to the total thermal conductivity in the corresponding direction, including both electron and phonon contributions.

In the case of Cr_2TiAlC_2, Seebeck coefficient in c direction is larger than that of a direction. The trend is reversed in Mo_2TiAlC_2 structure. This is mainly due to the different electronic structures of them in M–K direction in Brillouin zone, i.e., metallic in former phase and semiconducting in latter structure. It has been shown that Seebeck coefficient is directly proportional to the electronic density of states at Fermi level [38]. For good thermoelectric materials, the typical magnitude of Seebeck coefficient is usually hundreds of μV/K, i.e., 200∼600 μV/K [24,27,39–42]. Neither Cr_2TiAlC_2 nor Mo_2TiAlC_2 is considered as a promising thermoelectric material. Both phases exhibit very small Seebeck coefficients (tens of μV/K). The predicted ZT values of them confirm the conclusion further. For single crystal, the ZT reaches the maximum value of 0.32 at 1400 K for Mo_2TiAlC_2, and that value for Cr_2TiAlC_2 is 0.125 at 1200 K. For comparison, the ZT value of the well-known thermoelectric material Bi_2Te_3 was reported as 0.80 [40] or 1.20 [27]. Polycrystalline sample has significantly smaller ZT value than that of single crystal. Overall, total thermal conductivity of Cr_2TiAlC_2 or Mo_2TiAlC_2 bulk phase is roughly one-order of magnitude larger than many thermoelectric materials (0.5∼2 W/m K) [27,42]. Meanwhile, those new quaternary phases also have small Seebeck coefficients. As a result, the thermoelectric performance is not prominent in their bulk phases.

Although, the thermoelectric parameters of both Cr_2TiAlC_2 and Mo_2TiAlC_2 are far less attractive for practical applications, the relatively high thermal and electrical conductivities ensure their possible usages as rotating electrical contacts and heat exchanger [1]. It is also known that MAX phases Ti_3AlC_2 and Ti_2AlC show excellent oxidation resistance due the formation of dense Al_2O_3 layer on the bulk surface. The addition of Mo and Cr could improve this desired property further, because Mo and Cr are also highly resistant to various acids and oxidants. MAX phases also exhibit the remarkable crack healing ability at high temperature [43]. Therefore, the bulk Cr_2TiAlC_2 and Mo_2TiAlC_2 might be used to fabricate the high temperature components in turbine engines and aerospace industries [44].

4. Conclusions

In summary, electrical and lattice thermal conductivities of two newly discovered ordered quaternary MAX phases Cr_2TiAlC_2 and Mo_2TiAlC_2 were calculated in a and c directions. Both conductivities show anisotropic properties. The anisotropy is stronger in lattice thermal conductivity than in electrical conductivity. The total thermal conductivity in c direction is dominated by electrical part. Meanwhile, lattice thermal conductivity plays the key role in the total thermal conductivity of a direction at low temperature, and the electrical part determines total value at high temperature. Thermoelectric properties (Seebeck coefficient and ZT value) were investigated for polycrystalline sample and single crystal of two structures. Their thermoelectric performance is well below that of typical thermoelectric materials (Bi_2Te_3) due to the high thermal conductivity and small Seebeck coefficient.

Acknowledgements

Y.F. Li is supported by the National Natural Science Foundation of China (51501139), the Science and Technology Project of Guangdong Province in China (2015B010122003, 2015B090926009). Y.C. Ding is financially supported by the Department of Science and Technology of Sichuan Province (2015GZ0198). First-principles calculations within VASP program were carried out on the Q.Y Chen's

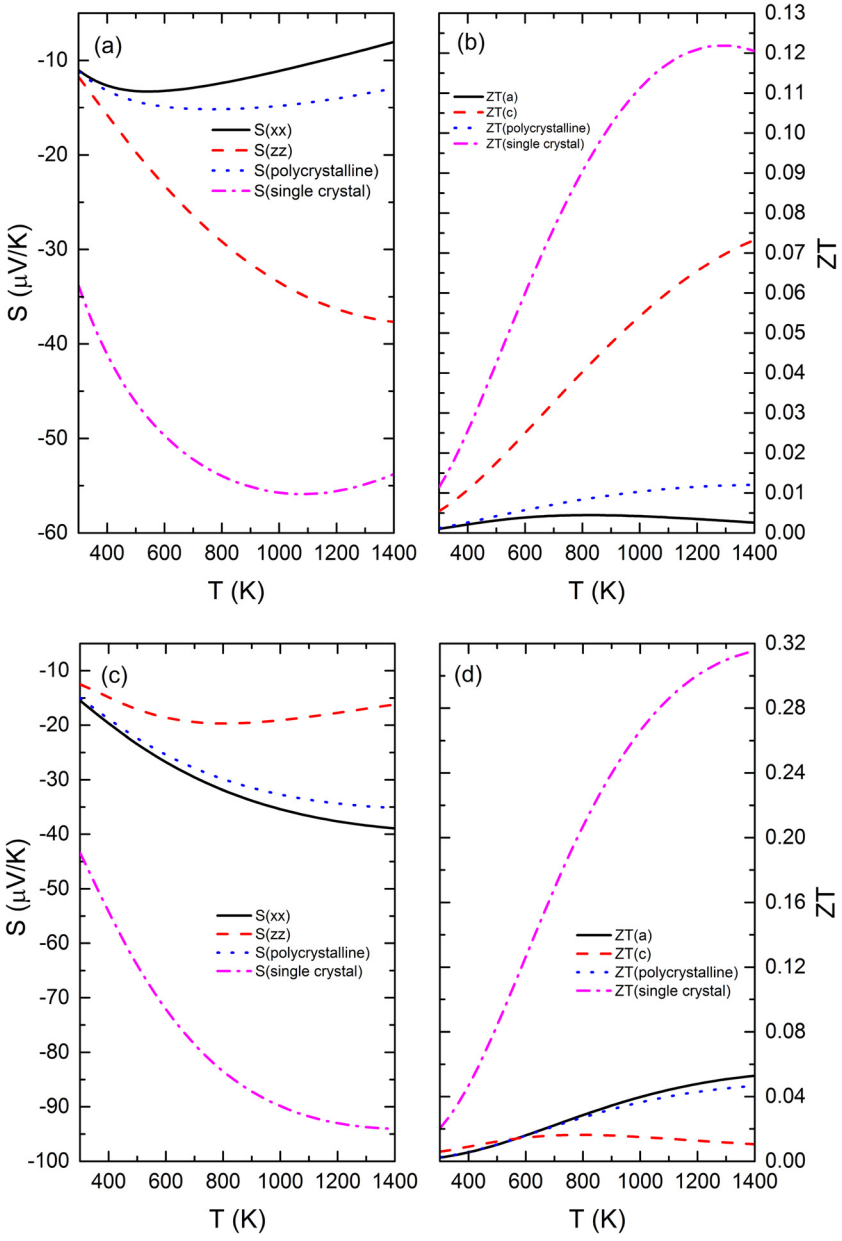

Fig. 8. Thermoelectric parameters as a function of temperature for Cr_2TiAlC_2 ((a) and (b)) and Mo_2TiAlC_2 ((c) and (d)). The Seebeck coefficients in *a*, *c* crystallographic directions, and for polycrystalline and single crystal are shown in (a) and (c). The thermoelectric figure of merit (ZT) is calculated in the similar way to Seebeck coefficient, and displayed in (b) and (d). Note that the negative sign of Seebeck coefficient implies the *n*-type conduction.

group clusters at the Southwest University of Science and Technology.

References

[1] M.W. Barsoum, M. Radovic, Annu. Rev. Mater. Res. 41 (2011) 195.
[2] M.W. Barsoum, H.I. Yoo, I.K. Polushina, V.Yu. Rud, Y.V. Rud, T. El-Raghy, Phys. Rev. B 62 (2000) 10194.
[3] M.W. Barsoum, T. El-Raghy, Am. Sci. 89 (2001) 334.
[4] X.H. Wang, Y.C. Zhou, Corros. Sci. 45 (2003) 891.
[5] X.H. Wang, Y.C. Zhou, J. Mater. Sci. Technol. 26 (2010) 385.
[6] Y.W. Bao, X.H. Wang, H.B. Zhang, Y.C. Zhou, J. Eur. Ceram. Soc. 25 (2005) 3367.
[7] M. Yoshida, Y. Hoshiyama, J. Ommyoji, A. Yamaguchi, Mater. Sci. Eng. B 173 (2010) 126.
[8] M.F. Cover, O. Warschkow, M.M.M. Bilek, D.R. McKenzie, Adv. Eng. Mater. 10 (2008) 935.
[9] Z. Liu, E. Wu, J. Wang, Y. Qian, H. Xiang, X. Li, Q. Jin, G. Sun, X. Chen, J. Wang, M. Li, Acta Mater. 73 (2014) 186.
[10] B. Anasori, J. Halim, J. Lu, C.A. Voigt, L. Hultman, M.W. Barsoum, Scr. Mater. 101 (2015) 5.
[11] B. Anasori, M. Dahlqvist, J. Halim, E.J. Moon, J. Lu, B.C. Hosler, E.N. Caspi, S.J. May, L. Hultman, P. Eklund, J. Rosen, M.W. Barsoum, J. Appl. Phys. 118 (2015) 094304.
[12] J. Zhang, Y.C. Zhou, J. Mater. Res. 23 (2008) 924.
[13] M. Naguib, M. Kurtoglu, V. Presser, J. Lu, J. Niu, M. Heon, L. Hultman, Y. Gogotsi, M.W. Barsoum, Adv. Mater. 23 (2011) 4248.
[14] M. Naguib, V.N. Mochalin, M.W. Barsoum, Y. Gogotsi, Adv. Mater. 26 (2013) 992.
[15] A.N. Enyashin, A.L. Ivanovskii, Comput. Theor. Chem. 989 (2012) 27.
[16] A.L. Ivanovskii, A.N. Enyashin, Russ. Chem. Rev. 82 (2013) 735.
[17] M.D. Segall, Philip J.D. Lindan, M.J. Probert, C.J. Pickard, P.J. Hasnip, S.J. Clark, M.C. Payne, J. Phys. Condens. Matter 14 (2002) 2717.
[18] H.J. Monkhorst, J.D. Pack, Phys. Rev. B 13 (1976) 5188.
[19] J.P. Perdew, K. Burke, M. Ernzerhof, Phys. Rev. Lett. 77 (1996) 3865.
[20] Grorg K.H. Madsen, D.J. Singh, Comput. Phys. Commun. 67 (2006) 175.
[21] G. Kresse, J. Furthmuller, Phys. Rev. B 54 (1996) 11169.
[22] J. Hafner, J. Comput. Chem. 29 (2008) 2044.
[23] P.E. Blochl, Phys. Rev. B 50 (1994) 17953.
[24] R. Guo, X. Wang, Y. Kuang, B. Huang, Phys. Rev. B 92 (2015) 115202.
[25] P.A. Burr, D. Horlait, W.E. Lee, Mater. Res. Lett., in press, http://dx.doi.org/10.1080/21663831.2016.1222598.
[26] Q.H. Gao, Z.J. Xu, L. Tang, X.J. Zuo, G.Z. Jia, A. Du, R.F. Linghu, Y.D. Guo, Z.J. Yang, Comput. Mater. Sci. 118 (2016) 77.

[27] P. Gorai, E.S. Toberer, V. Stevanovic, J. Mater. Chem. A 4 (2016) 11110.
[28] B. Peng, H. Zhang, H. Shao, Y. Xu, X. Zhang, H. Zhu, RSC Adv. 6 (2016) 5767.
[29] G.A. Slack, J. Phys. Chem. Solids 34 (1973) 321.
[30] C.L. Julian, Phys. Rev. 137 (1965) A128.
[31] L. Lindsay, D.A. Broido, T.L. Reinecke, Phys. Rev. B 87 (2013) 165201.
[32] A. Togo, L. Chaput, I. Tanaka, Phys. Rev. B 91 (2015) 094306.
[33] Y. Ding, M. Chen, B. Xiao, RSC Adv. 6 (2016) 7817.
[34] E.S. Toberer, A. Zevalkink, G.J. Snyder, J. Mater. Chem. 21 (2011) 15843.
[35] C. De Tomas, A. Cantarero, A.F. Lopeandia, F.X. Alvarez, J. Appl. Phys. 115 (2014) 164314.
[36] E.S. Toberer, A. Zevalkink, G.J. Snyder, J. Mater. Chem. 21 (2011) 15843.
[37] G.A. Slack, Solid State Phys. 34 (1979) 1.
[38] N.E. Mott, E.A. Davis, Electronic Processes in Non-crystalline Materials, second edition, Oxford University Press, 1979.
[39] D. Bayerl, E. Kioupakis, Phys. Rev. B 91 (2015) 165104.
[40] B. Sun, Z. Ma, C. He, K. Wu, Phys. Chem. Chem. Phys. 17 (2015) 29844.
[41] S. Bhattacharya, R. Chmielowski, G. Dennler, G.K.H. Madsen, J. Mater. Chem. A 4 (2016) 11086.
[42] D.B. Luo, Y.X. Wang, Y.L. Yan, G. Yang, J.M. Yang, J. Mater. Chem. A 2 (2014) 15159.
[43] G.M. Song, Y.T. Pei, W.G. Sloof, S.B. Li, J.T.M. De Hosson, S. Van der Zwaag, Scr. Mater. 58 (2008) 13.
[44] W.G. Sloof, R. Pei, S.A. McDonald, J.L. Fife, L. Shen, L. Boatemaa, A.S. Farie, K. Yan, X. Zhang, S. van der Zwagg, P.D. Lee, P.J. Withers, Sci. Rep. 6 (2016) 23040.